UNIVERSITY OF BIRMINGHAM
University of Birmingham Research at Birmingham

n-body dynamics of intermediate mass-ratio inspirals in star clusters

Haster, Carl-Johan; Antonini, Fabio; Kalogera, Vicky; Mandel, Ilya

DOI:
10.3847/0004-637X/832/2/192

License:
None: All rights reserved

Document Version
Publisher's PDF, also known as Version of record

Citation for published version (Harvard):
Haster, C-J, Antonini, F, Kalogera, V & Mandel, I 2016, '*n*-body dynamics of intermediate mass-ratio inspirals in star clusters', *The Astrophysical Journal*, vol. 832, no. 2. https://doi.org/10.3847/0004-637X/832/2/192

Link to publication on Research at Birmingham portal

General rights
Unless a licence is specified above, all rights (including copyright and moral rights) in this document are retained by the authors and/or the copyright holders. The express permission of the copyright holder must be obtained for any use of this material other than for purposes permitted by law.

•Users may freely distribute the URL that is used to identify this publication.
•Users may download and/or print one copy of the publication from the University of Birmingham research portal for the purpose of private study or non-commercial research.
•User may use extracts from the document in line with the concept of 'fair dealing' under the Copyright, Designs and Patents Act 1988 (?)
•Users may not further distribute the material nor use it for the purposes of commercial gain.

Where a licence is displayed above, please note the terms and conditions of the licence govern your use of this document.

When citing, please reference the published version.

Take down policy
While the University of Birmingham exercises care and attention in making items available there are rare occasions when an item has been uploaded in error or has been deemed to be commercially or otherwise sensitive.

If you believe that this is the case for this document, please contact UBIRA@lists.bham.ac.uk providing details and we will remove access to the work immediately and investigate.

Download date: 04. May. 2023

The Astrophysical Journal, 832:192 (11pp), 2016 December 1 doi:10.3847/0004-637X/832/2/192
© 2016. The American Astronomical Society. All rights reserved.

N-BODY DYNAMICS OF INTERMEDIATE MASS-RATIO INSPIRALS IN STAR CLUSTERS

Carl-Johan Haster[1,2], Fabio Antonini[2], Vicky Kalogera[2], and Ilya Mandel[1]
[1] School of Physics and Astronomy, University of Birmingham, Edgbaston, Birmingham B15 2TT, UK; cjhaster@star.sr.bham.ac.uk
[2] Center for Interdisciplinary Exploration and Research in Astrophysics (CIERA) & Dept. of Physics and Astronomy, 2145 Sheridan Rd, Evanston, IL 60208, USA
Received 2016 June 17; revised 2016 September 28; accepted 2016 September 29; published 2016 December 1

ABSTRACT

The intermediate mass-ratio inspiral of a stellar compact remnant into an intermediate-mass black hole (IMBH) can produce a gravitational wave (GW) signal that is potentially detectable by current ground-based GW detectors (e.g., Advanced LIGO) as well as by planned space-based interferometers (e.g., eLISA). Here, we present results from a direct integration of the post-Newtonian *N*-body equations of motion describing stellar clusters containing an IMBH and a population of stellar-mass black holes (BHs) and solar-mass stars. We take particular care to simulate the dynamics closest to the IMBH, including post-Newtonian effects up to an order of 2.5. Our simulations show that the IMBH readily forms a binary with a BH companion. This binary is gradually hardened by transient three-body or four-body encounters, leading to frequent substitutions of the BH companion, while the binary's eccentricity experiences large-amplitude oscillations due to the Lidov–Kozai resonance. We also demonstrate suppression of these resonances by the relativistic precession of the binary orbit. We find an intermediate mass-ratio inspiral in 1 of the 12 cluster models we evolved for ∼100 Myr. This cluster hosts a $100M_{\odot}$ IMBH embedded in a population of 32 $10M_{\odot}$ BH and 32,000 $1M_{\odot}$ stars. At the end of the simulation, after ∼100 Myr of evolution, the IMBH merges with a BH companion. The IMBH–BH binary inspiral starts in the eLISA frequency window ($\gtrsim$1 mHz) when the binary reaches an eccentricity $1-e\simeq 10^{-3}$. After $\simeq 10^{5}$ yr the binary moves into the LIGO frequency band with a negligible eccentricity. We comment on the implications for GW searches, with a possible detection within the next decade.

Key words: black hole physics – gravitation – gravitational waves

1. INTRODUCTION

Intermediate-mass black holes (IMBHs) are conjectured to occupy the mass range between stellar-mass black holes (BHs), with masses $\lesssim 100M_{\odot}$, and supermassive BHs with masses $\gtrsim 10^{6}M_{\odot}$ (see Miller & Colbert 2004, for a review). While the existence of some IMBH candidates in dwarf spheroidal galaxies has been conjectured by extending the M–σ relation (Graham & Scott 2013; but see Maccarone & Servillat 2008), dynamical measurements of IMBHs in the few-hundred solar-mass range are extremely challenging (e.g., Pasquato et al. 2016). The best evidence for such lower mass IMBHs (with mass $\sim 100M_{\odot}$) could come from ultraluminous X-ray sources (but see Berghea et al. 2008); for example, Pasham et al. (2014) have claimed a mass of ∼400 $M_{\odot}$ for M82 X-1 from quasi-periodic oscillations, while a mass around $10^{4}M_{\odot}$ has been suggested for the brightest ultra-luminous X-ray source HLX-1 (e.g., Farrell et al. 2009; Davis et al. 2011; Godet et al. 2014), but these dynamical measurements alone cannot provide conclusive proof for the existence of IMBHs.

If these lower mass IMBHs reside in star clusters, they will play an important role in cluster dynamics (e.g., Baumgardt et al. 2004a, 2004b; Trenti et al. 2010; Konstantinidis et al. 2013; Umbreit & Rasio 2013; Leigh et al. 2014; MacLeod et al. 2016). Of particular interest to our study is the likely tendency of IMBHs to dynamically form compact binaries with other compact remnants (e.g., Taniguchi et al. 2000; Miller 2002; Miller & Hamilton 2002; Amaro-Seoane & Freitag 2006; Brown et al. 2007; Mandel et al. 2008; Amaro-Seoane & Santamaría 2010; Mapelli et al. 2010; Mapelli 2016). Generally, these analyses find that the IMBH readily captures a binary companion. The binary is subsequently hardened through a sequence of three-body and four-body interactions, occasionally with substitutions that make a BH of a few tens of solar masses the most likely IMBH companion, and possible Lidov–Kozai (LK) resonances (Lidov 1962; Kozai 1962) if hierarchical triples are formed. Eventually, the IMBH–BH binary merges through the radiation of gravitational waves (GW), emitting a signal that is potentially detectable by the Advanced LIGO ground-based GW detectors (Abadie et al. 2010; Smith et al. 2013; Aasi et al. 2015; Haster et al. 2016).

Previous simulations of star clusters with IMBH coalescences have generally simplified the interactions in order to avoid excessive computational cost. For example, Gültekin et al. (2004) considered a series of individual Newtonian interactions interspersed with orbital evolution through GW emission. Mandel et al. (2008) carried out analytical estimates of the hardening sequence to obtain the intermediate mass-ratio merger timescale. Leigh et al. (2014) simulated the entire cluster with a mixture of analytical and numerical *N*-body analytical calculations, while MacLeod et al. (2016) focused their *N*-body investigation on tidal disruptions of stars by the IMBH as well as merger events. We note that in the previous literature effects of pN terms are either not accounted for (Leigh et al. 2014), or included only at the 2.5pN level (Samsing et al. 2014; MacLeod et al. 2016). In this paper we show a clear example in which lower order pN terms play a fundamental role in the dynamics. More specifically, an essential element that differs between the relativistic and non-relativistic dynamics turns out to be the 1pN precession of the periapsis.

We introduce our numerical method and the simulation setup in Section 2. We describe our simulation results in Section 3. We discuss the results, including the detectability of GWs from intermediate mass-ratio coalescences, in Section 4.

2. SIMULATIONS

The N-body systems considered here consist of a massive particle, representing an IMBH, and two additional lower mass species representing $10M_{\odot}$ compact remnants and $1M_{\odot}$ stars. Integrations of the N-body equations of motion were carried out using the direct summation N-body code phiGRAPEch (Harfst et al. 2008). This code incorporates Mikkola's algorithmic chain regularization scheme including post-Newtonian terms of order 1pN, 2pN, and 2.5pN (AR-CHAIN, Mikkola & Merritt 2008). Velocity-dependent forces were included using the generalized midpoint method described by Mikkola & Merritt (2006). The algorithm produces exact trajectories for Newtonian two-body motion and regular results for strong encounters involving arbitrary numbers of bodies. Particles moving beyond the "chain radius" ($r_{\rm chain}$) were advanced using a fourth-order integrator with forces computed on GPUs using the Sapporo library (Gaburov et al. 2009). The chain particles were influenced by the global cluster dynamics through the particles in a perturber region, within a radius $r_{\rm perturb}$ from the IMBH. phiGRAPEch is an ideal tool for the study of the dynamics of IMBHs in star clusters because it allows us to study with extremely high precision the joint effect of 1pN, 2pN, and 2.5pN terms and their interplay with Newtonian perturbations to the motion.

We performed 12 simulations, all initialized as a King model with no primordial binaries, containing two mass species (BHs and stars) with a relative mass ratio of 10:1, and assuming that the total mass in BHs is 1% of the total cluster mass. Finally, an initially stationary IMBH was placed at the center of the cluster. The analytical King model was chosen because, despite its dynamical simplicity, it provides a good fit to observed surface brightness profiles. King models are defined as approximate iso-thermal spheres with a modified density profile such that the energy, as well as the number density, decreases with radius until it becomes zero at the tidal radius $r_{\rm t}$. Together with the King radius

$$r_0 \equiv \sqrt{\frac{9\sigma^2}{4\pi G\rho_0}} \tag{1}$$

where σ is the velocity dispersion of the cluster and ρ_0 is its central density, this defines the concentration parameter $W_0 \equiv r_{\rm t}/r_0$ ($W_0 = 7$ for all our simulations). The simulations were performed with number of particles $N \subset \{32768, 65536\}$ IMBH mass, $M \subset \{50, 100, 200\}\ M_{\odot}$, and cluster virial radius r_v defined as

$$\frac{M_{\rm tot}^2}{r_v} \equiv \sum_{i=0}^{N}\sum_{j\neq i}^{N}\frac{m_i m_j}{|\boldsymbol{r}_i - \boldsymbol{r}_j|} \tag{2}$$

given the cluster total mass $M_{\rm tot}$, and particle masses and distances m and $\boldsymbol{r}$ summed over all particle pairs i, j. r_v was in these simulations set as 3.5 pc, which in turn gave $r_v \sim 5r_0$ for our choice of King models. For $N = 32{,}768$ and all three IMBH masses, simulations with $r_v \subset \{0.35, 1.0\}$ pc were also performed. The inclusion of high-order pN terms fixes the physical scale of the cluster, thus removing the conventional freedom for rescaling simulations in cluster size and density.

We observe the IMBH forming a binary with a BH within $\lesssim$20 Myr in every simulated cluster; this can be compared to the relaxation time for the cluster core of $\sim$6 Myr. Only in one cluster ($N = 32768$, $M = 100M_{\odot}$, $r_v = 3.5$ pc) do we observe a merger within the simulated time ($\simeq$100 Myr). While the result of the entire set of simulations will be presented in a future paper, in what follows we will focus on describing the detailed dynamics of the one cluster producing the merger event. We note in passing that as the main focus of this study is the dynamical formation and evolution of binaries, and higher order N-tuples, with the IMBH as the primary companion, all cluster particles are solely characterized by their mass and no stellar evolution is included in these simulations. The effects of natal kicks in the formation of the BHs, and any eventual ejections of BHs from the cluster that these kicks might cause, have also been excluded in these simulations (cf. Morscher et al. 2015).

3. RESULTS

The simulated star cluster was initialized with the IMBH at rest at the center while the remaining stars and BHs follow a King model. Figure 1 shows the position of the IMBH and a subset of BH particles, and their subsequent movement within the cluster, relative to the center of mass of the entire cluster. This subset of the BH population were those that were ejected from the cluster during the simulation. Although the IMBH is initially at rest at the cluster center of mass, it quickly experiences significant Brownian motion within a sphere of radius $\sim$0.1 pc around the center of mass to be compared to the core radius of $\sim$0.7 pc. The typical distance wandered by the IMBH in the core is larger than the radius of influence of the IMBH.

Shifting the focus from the global dynamical behavior within the cluster, Figure 2 displays the time evolution of the relative distance to the IMBH of those BHs that experienced close encounters with the IMBH at some point of the simulation. In this figure we see that while the IMBH is interacting only weakly with its surroundings at the start of the simulation, after $\sim$3 Myr it forms a wide binary with a stellar particle, and after $\sim$25 Myr the binary companions are BHs, consistent with the expected mass segregation in this cluster. By comparing the ejected BHs between Figures 1 and 2 it is clear that after the first few ejected BHs (which were driven by their initially relatively high kinetic energy and interactions with other cluster members) and following the formation of the IMBH–BH binary, all subsequent ejections are driven by interactions with the IMBH–BH binary. These interactions lead to the frequent substitution of the IMBH binary companion, with three out of the five observed substitution events leading to the former companion being ejected from the cluster. The remaining two were returned to the cluster BH population, where one BH ($\rm BH_B$ in Figures 1 and 2) was later recaptured by the IMBH. Figure 2 also shows the transient three-body interactions, such as the ejection of $\rm BH_F$, and their effectiveness in the continued hardening of the IMBH–BH binary. The behavior shown in Figure 2 is similar to the results in MacLeod et al. (2016), e.g., from their Figure 1, which also shows a prompt aquisition of a binary partner to the IMBH and subsequent exchange of companion until the binary is terminated.

The time evolution of this binary is most clearly visualized in terms of its orbital parameters where Figure 3 shows the IMBH–BH binary semimajor axis.[3] Once the IMBH captures a stellar-mass BH companion, the IMBH–BH binary is hardened

[3] The semimajor axes and eccentricities were computed using the post-Newtonian formalism given in Equation (3.6) of Damour & Deruelle (1985).

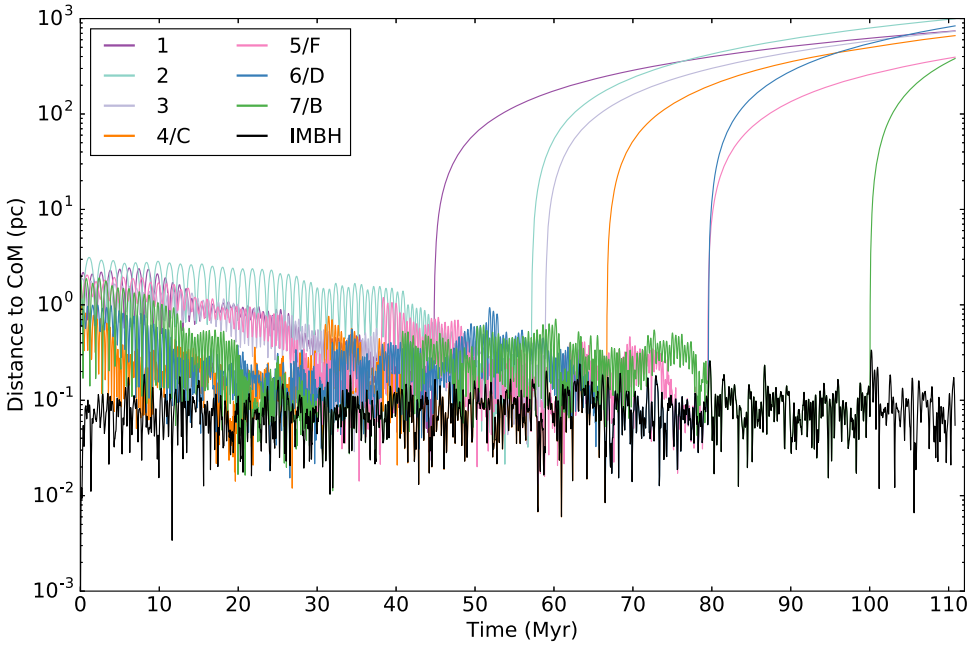

Figure 1. Time evolution of the distance of the IMBH (in black) to the center of mass (CoM) of the entire cluster. The IMBH wanders throughout the simulation within a central region extending to $\lesssim$0.1 pc around the cluster CoM, compared to the core radius of ~0.7 pc. Also shown (in color) are the BHs that were ejected from the cluster and the corresponding time of ejection. BHs for which we have assigned both a numerical and alphabetical index were bound to the IMBH before being ejected from the cluster. The evolution of the orbits of these BHs is also shown in Figure 2.

by three-body interactions (see Section 3.5 of MacLeod et al. 2016). The hardening of the binary is clearly visible in Figure 3 as the semimajor axis of the IMBH–BH binary decreases monotonically, with the jumps in semimajor axis being signs of energetic three-body interactions. While Figure 2 only shows the BH interactions, there are also a multitude of stellar transient passes carrying energy away from the IMBH–BH binary.

Gravitationally focused interactions, which approach the hard IMBH binary within its semimajor axis a_i, happen on a typical timescale (e.g., Mandel et al. 2008)

$$\tau_{\text{3-body}} \simeq 5 \times 10^7 \left(\frac{100 M_\odot}{M_b}\right)\left(\frac{v}{10\ \text{km s}^{-1}}\right) \times \left(\frac{10^{5.5}\ \text{pc}^{-3}}{n}\right)\left(\frac{0.05\ \text{au}}{a_i}\right) \text{year}, \quad (3)$$

where M_b is the binary's mass (dominated by the IMBH), v is the velocity dispersion in the cluster, and n is the number density of stars and BHs in the cluster center. The binary hardens through three-body interactions on the typical timescale (e.g., Quinlan 1996; Mandel et al. 2008)

$$\tau_{\text{harden}} \simeq \frac{22}{\pi}\frac{M_b}{m_*}\tau_{\text{3-body}}, \quad (4)$$

where m_* is the interloper mass. Following Antonini & Rasio (2016) we define a_{ej} as the binary semimajor axis below which a three-body interaction will cause the binary to be ejected from the cluster:

$$a_{ej} \simeq 0.2 G\mu \frac{m_*}{M_b + m_*}\frac{m_*}{M_b}\frac{1}{v_{\text{esc}}^2} \quad (5)$$

where $\mu = Mm/(M+m)$ for M is the IMBH mass, m is the mass of its BH companion, and v_{esc} is the escape velocity from the core of the cluster. As the binary hardens, after $\simeq$110 Myr the time to the next interaction drops below the GW-driven merger timescale, which, in the limit of large binary eccentricities, is approximated by (Peters 1964)

$$\tau_{\text{merge}} \simeq 3 \times 10^7 \left(\frac{10^5 M_\odot^3}{M^2\, m}\right)\left(\frac{a_i}{0.05\ \text{au}}\right)^4 (1 - e_i^2)^{7/2}\ \text{year}, \quad (6)$$

where e_i is the IMBH–BH binary eccentricity. The semimajor axis a_{GW} at which the evolution of the binary starts to be dominated by GW radiation, and no further significant three-body interactions are expected, can be found by setting

$$\tau_{\text{merge}} = \tau_{\text{3-body}}, \quad (7)$$

which gives

$$a_{\text{GW}} \simeq \frac{0.12}{(1 - e_i^2)^{7/10}}\ \text{au}, \quad (8)$$

with $M = 100 M_\odot$, $m = 10 M_\odot$, $n = 5 \times 10^3\ \text{pc}^{-3}$, and $v = 10\ \text{km s}^{-1}$ reflecting the cluster center at the time of the merger onset seen in Figure 3. At separations below a_{GW} the evolution of the binary is dominated by energy loss due to GW emission and for $a_{\text{GW}} > a_{ej}$ the merger will occur before the binary will be ejected from a three-body interaction.

Mandel et al. (2008) computed the total time to IMBH–BH coalescence by summing the hardening time to the last interaction with the subsequent merger timescale under the assumption that the last interaction is likely to leave the binary with an eccentricity of $\simeq$0.98 (Gültekin et al. 2006). However, as shown in what follows, even higher eccentricities can be reached during the complex three-body interactions, possibly reducing the merger timescale (Antonini et al. 2014; Samsing et al. 2014).

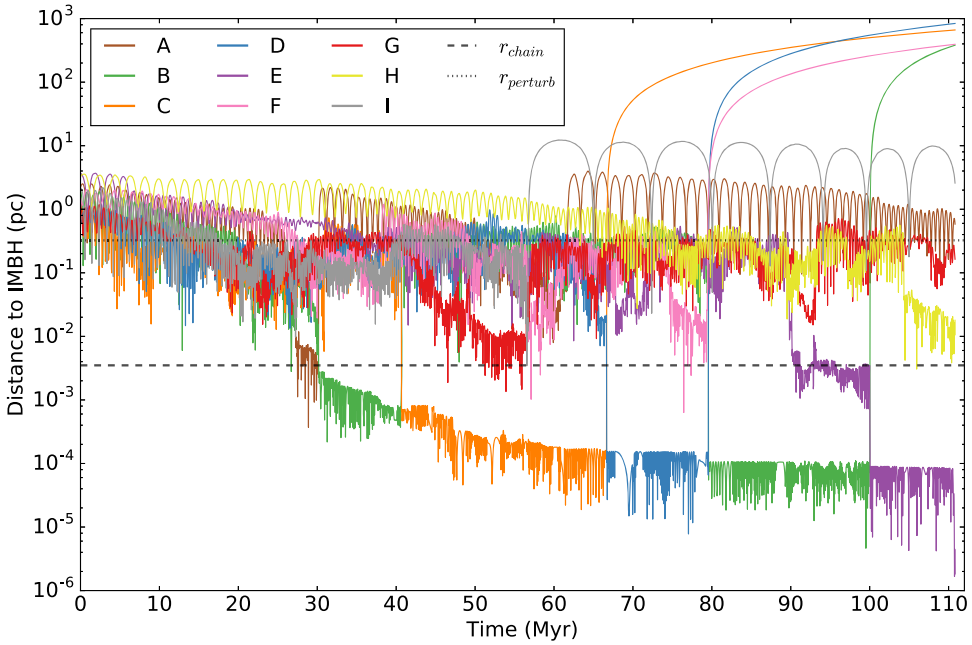

Figure 2. Distance to the IMBH vs. time for BHs, which at any point in the simulation came within 4 mpc of the IMBH. Within the first 3 Myr the IMBH acquires a binary companion, at first a stellar particle which is substituted for a BH companion at ∼25 Myr, in this case BH_A, forming a wide binary. Through interactions with other objects embedded in the cluster potential this binary is hardened. The IMBH–BH binary undergoes many companion substitutions, often while in hierarchical N-tuples, resulting in both later recaptures (BH_B) and ejections from the cluster ($BH_{C,D,B}$). The dashed black line marks the transition distance $r_{\rm chain}$ below which the dynamics are treated by AR-CHAIN under the gravitational influence of all perturbing particles within the region represented by the dotted black line ($r_{\rm perturb}$).

Figure 4 shows the evolution of the binary eccentricity (top panel) and the inclination of the outer to the inner binary when the binary is part of a triple system (ι_0; bottom panel). The complex dynamical structure of the surroundings of the binary, including both stellar and BH interactions, is evident in Figure 4 where large-amplitude variations of the IMBH–BH binary eccentricity are observed. The evolution of e_i and ι_0 is driven both by transient passes and by longer duration LK and post-Newtonian effects.

The eccentricity oscillations in hierarchical triple systems can potentially drive up the eccentricity of the inner binary to very high values, possibly leading to faster GW-driven mergers (Miller & Hamilton 2002; Aarseth 2012; Antonini et al. 2014). The timescale for a full oscillation in eccentricity is given as

$$\mathrm{T_{LK}} \simeq \frac{P_i}{2\pi}\frac{M+m}{m_o}\left(\frac{a_o}{a_i}\right)^3(1-e_o^2)^{3/2} \tag{9}$$

where a_i, a_o are the semimajor axes of the inner and outer binary, respectively (within the hierarchical triple system), e_o is the eccentricity of the outer orbit, m_0 is the mass of the tertiary BH, and $P_i = 2\pi\sqrt{a_i^3/G(M+m)}$ is the orbital period of the inner binary (Holman et al. 1997). We also define here a dimensionless angular momentum as the angular momentum of the binary divided by the angular momentum of a circular orbit with the same semimajor axis: $\ell_i = \sqrt{1-e_i^2}$; this is a useful quantity when discussing LK oscillations, as they do not affect the orbital energy. The timescale over which the inner binary changes the value of its angular momentum by the order of itself is then (Bode & Wegg 2014; Antonini et al. 2016a)

$$\tau_{\rm LK} \equiv \left|\frac{1}{\ell_i}\frac{d\ell_i}{dt}\right|^{-1}_{\rm LK} \simeq T_{\rm LK}\sqrt{1-e_i^2}, \tag{10}$$

directly related to the period of the LK oscillation.

At the quadrupole level of approximation and in the test particle limit, for an orbit librating around the argument of periapsis $\omega_i = \pi/2$, the maximum (ℓ_+) and minimum (ℓ_-) angular momenta during a LK cycle are related through the equation (e.g., Merritt 2013)

$$\ell_+\ell_- = \sqrt{\frac{5}{3}}\ell_z. \tag{11}$$

In the previous expression $\ell_z = \ell_i\cos\iota_0$ is a conserved quantity for an initial orbital inclination ι_0 in the quadrupolar limit. From Equation (11), and from the conservation of ℓ_z one finds that the maximum eccentricity that can be attained during a LK cycle is simply $e_{\rm max} = \sqrt{1-(5/3)\cos^2\iota_0}$ (Innanen et al. 1997).

Post-Newtonian corrections to the orbital dynamics can affect the binary on similar timescales as $\tau_{\rm LK}$, where the most prominent effect would be the 1pN Schwarzschild precession (SP) of the argument of periapsis ω_i. To lowest order, the timescale associated with SP is

$$\tau_{\rm SP} \equiv \left|\frac{1}{\pi}\frac{d\omega_i}{dt}\right|^{-1}_{\rm SP} \simeq \frac{P_i}{6}\frac{a_i}{r_g}(1-e_i^2) \tag{12}$$

with $r_g = G(M+m)/c^2$. When SP is considered, Equation (11) becomes (Antonini et al. 2016b)

$$\ell_+^2\ell_-^2 = \frac{5}{3}\ell_z^2 + \frac{k}{3}\left(\frac{\ell_+-\ell_-}{\ell_+^2-\ell_-^2}\right)\ell_+\ell_-, \tag{13}$$

with

$$k = 8\frac{M}{m}\frac{r_g a_o^3}{a_i^4}(1-e_o^2)^{3/2}. \tag{14}$$

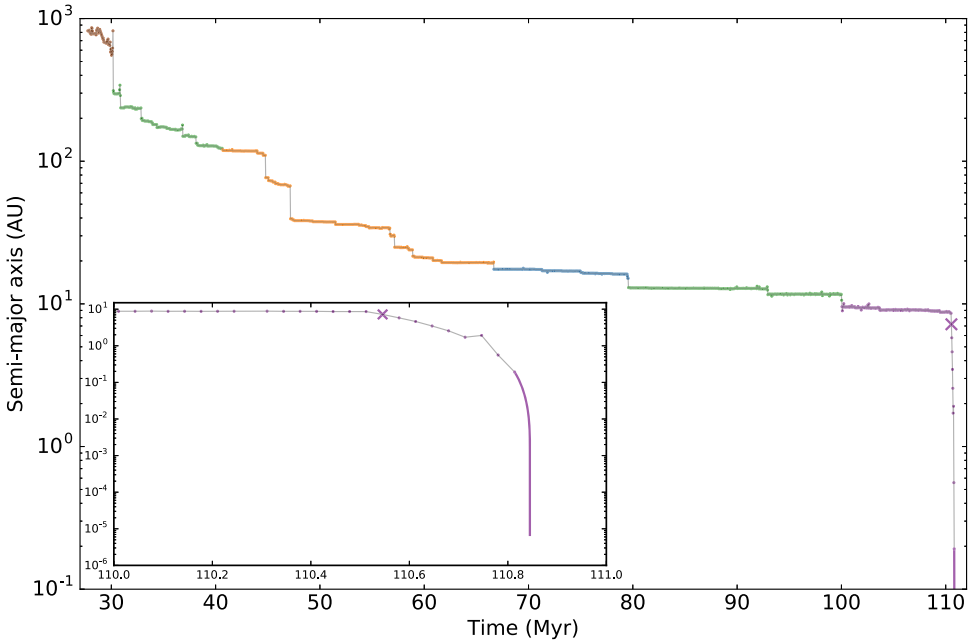

Figure 3. Binary consisting of an IMBH and another BH will harden over time and lose energy to its surroundings, manifested by the shrinking of the binary's semimajor axis through a series of parthership exchanges. The colors match Figure 2 to highlight the substitution of the binary companions. At the end of the simulation the IMBH, through external perturbation by BH_H, is set on a trajectory toward a merger with its binary companion BH_E while still inside the cluster. The point where GW emission becomes dominant in the orbital evolution (see Equation (8)) is marked by a purple $\times$. At the end of the simulation the binary orbit is evolved until merger according to Peters (1964), marked by the solid purple line; this is further highlighted in the inset figure showing the last Myr before merger.

This shows that SP effects can suppress the phase space available for libration for systems with $\tau_{\rm SP} < \tau_{\rm LK}$, reducing the maximum eccentricity attained during an LK cycle. In fact, from Equation (13), given that the second term on the right-hand side of the equation is always positive, we see that for a given ℓ_+ SP will lead to an increase of ℓ_-.

By setting $\tau_{\rm LK} = \tau_{\rm SP}$ we find the critical angular momentum

$$\ell_{\rm SP} \sim \frac{r_g}{a_i}\frac{M+m}{m_o}\left(\frac{a_o}{a_i}\right)^3, \tag{15}$$

which in turn can be represented as an eccentricity boundary $e_{\rm SP} = \sqrt{1-\ell_{\rm SP}^2}$ to the eccentricities within reach of LK oscillations. SP will dominate the orbital evolution of the inner binary at eccentricities larger than $e_{\rm SP}$, thus quenching the possibility of eccentricity oscillations caused by LK resonance. When $\ell_{\rm SP} \gtrsim 1$, then SP will dominate over the torque from the outer tertiary BH for any value of e_i and LK oscillations are expected to be fully suppressed. In Figure 4 we show when this happens using a solid red line at $\ell_{\rm SP} = 1$. As expected, no LK oscillations occur when $\ell_{\rm SP} \gtrsim 1$. In Figure 4 the $e_{\rm SP}$ boundary is shown only when there is a hierarchical triple system present, with the IMBH–BH binary at its center. During the periods of active LK oscillations, for example between $\sim$90 and 100 Myr, it is clear that the eccentricity of the IMBH–BH binary never exceeds the $e_{\rm SP}$ boundary. This is further evidence that SP plays a fundamental role in the dynamical evolution of the IMBH–BH binary in our simulations. The detailed interaction between LK and SP dynamical effects is also discussed by Naoz et al. (2013) who find that, assuming Newtonian dynamics to octupolar order with an added 1pN (only) correction term, SP in hierarchical triples can excite eccentricity rather than suppress it for $\tau_{\rm SP} \sim \tau_{\rm LK}$. While qualitatively similar behavior can be observed in our simulation, it is difficult to distinguish effects like this from other mechanisms subdominant to the LK oscillations (e.g., the hierarchical mass-ratio configuration, stellar interlopers, and the perturbing cluster potential) without further investigation.

In addition to LK suppression from relativistic precession, the presence of strong Newtonian precession, induced by the IMBH–BH binary existing within a dynamical cluster, would have similar effects on the binary orbital evolution. We find the classical precession to be negligible compared to SP for the periods when the IMBH–BH binary is in a hierarchical triple, and thus has no effect on the LK suppression caused by precession of the IMBH–BH orbit.

Between $\sim$90 and 93 Myr we find that the IMBH–BH binary is part of a hierarchical quadruple BH (IMBH, BH_B, BH_E, BH_F), with a resolved two-level LK oscillation. As discussed by Hamers et al. (2015), as the individual $\tau_{\rm LK}$ for the two LK systems are comparable, this induces complex LK oscillations in the IMBH–BH binary, further enhancing the transfer of angular momentum away from it. This is most clearly exemplified by the eccentricity: the expected maximum eccentricity $e_{\rm max} \simeq 0.3$ from $\iota_0 = 43\overset{\circ}{.}1$ at 90 Myr is substantially smaller than the eccentricities achieved during the existence of the quadruple BH. It is also interesting to note that the two LK timescales associated with the quadruple are both below the corresponding $\tau_{\rm SP}$ for the inner binary as well as the empirical timescale for the precession of ω_i induced by the presence of the quadruple within the stellar cluster. Eventually at $\simeq$93 Myr the quadruple system is disrupted by the removal of the outermost BH. At 93–100 Myr of evolution the eccentricity of the IMBH–BH binary clearly undergoes large-amplitude LK oscillations as expected given the high mutual inclination of the outer to inner orbit ($\iota_0 = 78\overset{\circ}{.}5$) at this time.

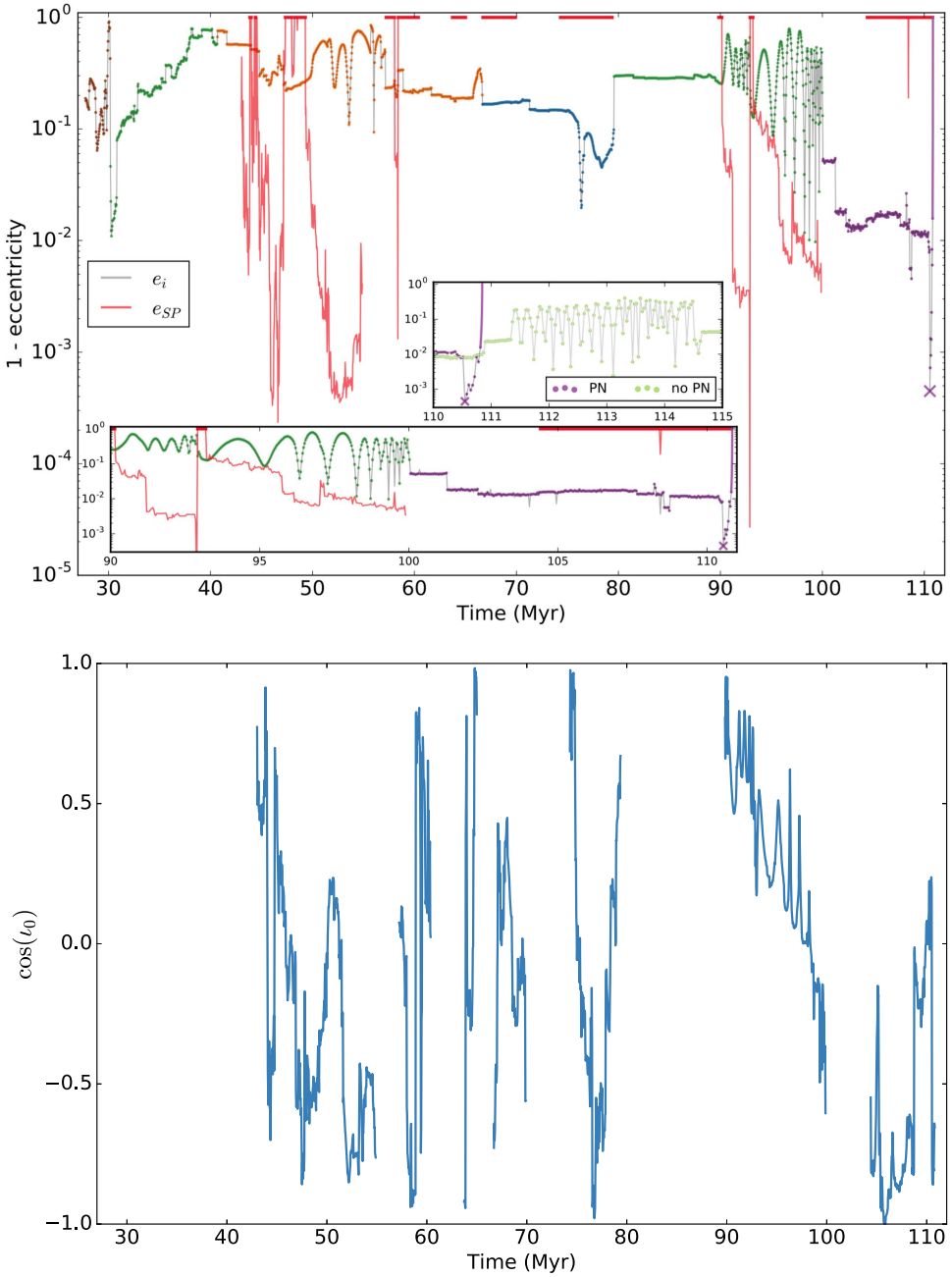

Figure 4. Evolution of the IMBH–BH binary eccentricity (top). The colors of e_i match those of Figure 2 to highlight the many substitutions of the binary companions. The figure shows clear evidence for both transient three-body interactions as well as longer timescale LK oscillations. For the majority of the binary's presence in a hierarchical N-tuple LK effects are suppressed by the SP of the inner binary orbit. The precession is represented here as an effective eccentricity boundary $e_{\rm SP}$ above which LK oscillations are suppressed (corresponding to *below* the $e_{\rm SP}$ line in this figure). The bottom inset shows the last ∼20 Myr exhibiting LK oscillations, bounded by $e_{\rm SP}$, in a quadruple and later a triple BH system ended by the substitution of the IMBH binary companion. This last binary configuration is frozen at high e_i, suppressed by SP and later merged. The point where the binary evolution is dominated by GW emission is marked by a purple ×. At the end of the simulation the binary orbit is evolved using the formula of Peters (1964) marked by the solid purple line. To further highlight the importance of the post-Newtonian dynamics the upper inset also includes a simulation (presented in light green) started at ∼1 Myr before the observed merger, but using only Newtonian dynamics. The clear eccentricity oscillations in a triple system where SP would have completely suppressed LK provide evidence for the importance of pN dynamics. Also shown in the bottom panel is the inclination ι_0 between the inner and outer orbits for the times when the IMBH exists in a bound triple system.

While the observed oscillations in eccentricity and inclination of the IMBH triple system show all signs of being caused by the LK mechanism, it is important to keep in mind that "pure" LK oscillations assume an isolated three-body system. Here we are able to observe (for the first time) this mechanism acting on a triple system embedded in a dynamically evolving stellar cluster while also accounting for relativistic corrections to the motion.

Also interesting are the regions where $e_{\rm SP} = 0$, or equivalently $\ell_{\rm SP} \geqslant 1$. Here the SP is dominating the IMBH–BH binary to such a degree that no eccentricity oscillations driven by LK are possible. We find that the inclination of the IMBH–BH binary relative to the outer BH orbit evolves stochastically, attaining at times values near 40°, which based on Equation (11) should lead to LK eccentricity oscillations with a period $\simeq 5 \times 10^6$ yr following Equation (9).

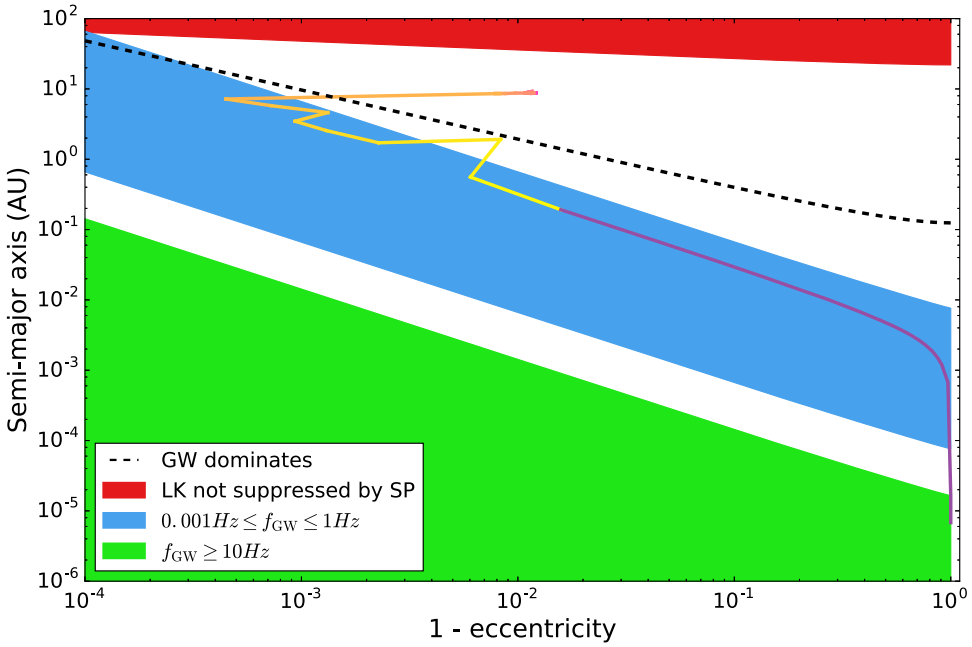

Figure 5. As the IMBH–BH binary evolves during its final Myr (time increases from red to yellow) it is frozen at very high eccentricities due to the suppression of LK oscillations by the SP of the IMBH–BH binary. The red region indicates where this suppression would be absent. The presence of a stable triple system, as indicated in Figure 2, causes perturbations of the IMBH orbit from both the tertiary BH_H and additional stellar interlopers. One of the stellar perturbations brings the three objects so close together that the IMBH–BH binary orbital evolution becomes dominated by emission of GWs. Additionally, this ejects the stellar interloper at a velocity $\sim$120 km s^{-1}. The limiting semimajor axes below which a three-body interaction with an interloper of mass m_* will eject the binary are shown as dotted and dash-dotted lines following Equation (5). GW emission dominates below the dashed black line, given by Equation (8); in this regime merger through the emission of GWs will occur before the next three-body interaction can significantly alter the IMBH–BH binary eccentricity, and thus its evolutionary timescale (see the interloper that initiated the merger trajectory). Much of the GW-dominated evolution occurs at GW frequencies observable by eLISA, as indicated by the blue region. As the IMBH–BH binary evolves along its merger trajectory there are still a small number of minor three-body encounters with stellar interlopers passing within a few semimajor axes of the binary CoM; these interactions are the cause of the "spikes" visible in the merger trajectory. These interactions are consistent with the timescales given in Equations (4) and (6), which predict that the last interaction before merger should occur when this system has a semimajor axis of $\sim$1 AU. At the end of the simulation the binary's orbit is evolved to merger, within the Advanced LIGO sensitive band (marked by the green region), according to Peters (1964), as shown by the purple line.

Contrary to this, during the last $\sim$10 Myr the IMBH–BH binary appears to be "frozen" at high e_i with SP suppressing any eccentricity reduction apart from the higher pN-order emission of GWs. After a strong interaction with a stellar interloper, which in turn is ejected from the cluster at $\sim$120 km s^{-1}, the loss of energy and angular momentum through GWs determines the ultimate fate of the binary, leading to its merger $\sim$300,000 yr later (see Figure 5).

During the initial GW-dominated phase, the binary experiences a small number of three-body interactions with stellar interlopers, which are the cause of the "spikes" visible in Figure 5. However, these interactions do not disrupt the binary inspiral and since they occur at $a_i > a_{ej}$, shown in Figure 5 for both possible interloper masses and $v_{\rm esc} = 9.9$ km s^{-1}, the interaction does not eject the binary from the cluster.

A highly eccentric binary emits a broad spectrum of gravitational radiation during each periapsis passage. We identify the frequency of the harmonic containing the maximal gravitational radiation as (Wen 2003)

$$f_{\rm GW} = \frac{\sqrt{G\,(M+m)}}{\pi}\frac{(1+e_i)^{1.1954}}{[a_i(1-e_i^2)]^{1.5}}; \qquad (16)$$

this is the GW frequency plotted in Figure 5.

The binary spends $\simeq$300,000 yr in the eLISA sensitive frequency window, which spans (0.001 Hz $\lesssim f_{\rm GW} \lesssim$ 1 Hz). Meanwhile, the last 6 s of the inspiral, followed by the merger and subsequent ringdown of the resulting IMBH, occur in the GW spectrum observable by Advanced LIGO ($f_{\rm GW} \gtrsim$ 10Hz). As suggested by Amaro-Seoane & Santamaría (2010) for IMBH–IMBH binaries and Abbott et al. (2016a) and Sesana (2016) for binary BH systems similar to the detected GW150914 (Abbott et al. 2016b), this type of IMBH–BH coalescences represents a class of GW sources potentially observable in both space- and ground-based detectors, providing an opportunity for long-term detailed studies of both their formation environments and probes of general relativity itself. We discuss the near-term prospects of detecting such binary mergers with Advanced LIGO in the following section.

To further verify the importance of the inclusion of the pN effects in our models, the simulation was restarted $\sim$1 Myr before the merger, removing all pN terms from the equations of motion. As shown by the light green samples in the upper inset of Figure 4, removing pN terms results in eccentricity oscillations without, of course, a GW-induced merger. During these oscillations the IMBH remains in a bound triple system (IMBH, BH_E, BH_H) in which SP would have been the dominant dynamical factor, completely removing the possibility for LK oscillations.

In addition, we performed one simulation, also started $\sim$1 Myr before the merger, where the chain regularization was disabled. In this simulation the surrounding N-body integrator could not accurately follow the very hard IMBH–BH binary; this had the effect of significantly slowing down the simulation while no longer adhering to the conservation of total energy within the cluster. This loss of $\frac{\Delta E}{E} \sim 0.01$ per time-step $\Delta t = 67$ kyr accumulates as the simulation progresses, to be

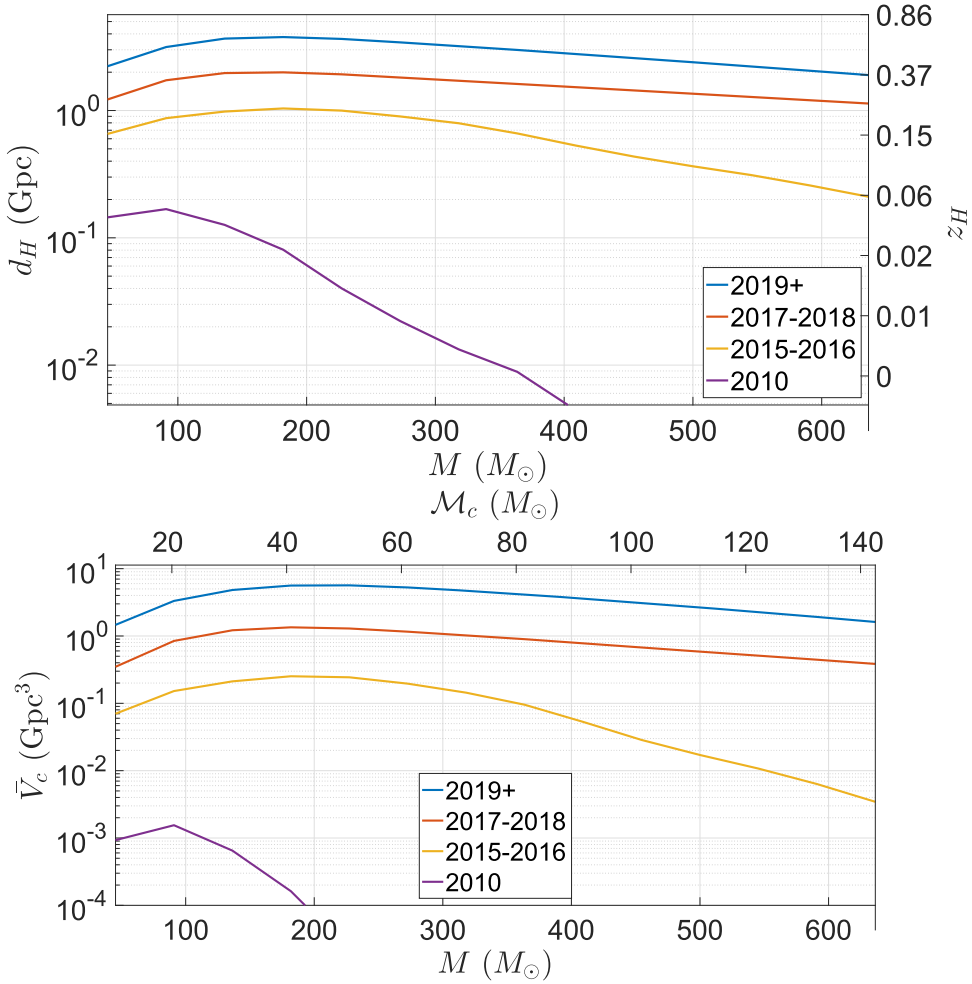

Figure 6. Top: horizon distance (left axis) and horizon redshift (right axis) as a function of IMBH mass for IMBH–BH coalescences with non-spinning components with a 10:1 mass ratio, for different detector sensitivities (see text). Bottom: detection-weighted sensitive comoving volume (Equation (17)); when multiplied by a constant merger rate per unit comoving volume per unit source time, this yields a detection rate.

compared with $\frac{\Delta E}{E} \sim 10^{-4}$ per time-step when including the chain regularization. These results further demonstrate the importance of using a high-accuracy integrator like ARCHAIN in order to study the evolution of IMBHs in cluster simulations.

4. DISCUSSION

GWs from intermediate mass-ratio coalescences are observable with both the advanced network of ground-based detectors (Aasi et al. 2015; Acernese et al. 2015) and a future space-based GW detector (eLISA Consortium 2013). The observed binary inspiral is in the eLISA sensitivity band throughout the circularizing phase. However, detection and parameter estimation at very high eccentricities could prove problematic without high-accuracy eccentric templates for matched filtering the bursts of radiation expected during the few periapsis passages over the lifetime of a space-borne mission (Amaro-Seoane et al. 2007; Porter & Sesana 2010; Key & Cornish 2011; Berry & Gair 2013). Both detection and parameter estimation would be more amenable to existing techniques later in the orbital evolution (Huerta et al. 2014; Moore et al. 2016; Nishizawa et al. 2016; Tanay et al. 2016; Tiwari et al. 2016), for $e_i \lesssim 0.1$ in Figure 5, and with only 10 yr from $e_i = 0.1$ until merger for this system a co-observing campaign together with ground-based detectors, where the system is effectively fully circularized, would be possible.

As discussed by Sesana (2016) and Vitale (2016) in relation to binary BHs similar to GW150914, the extended observation in eLISA would provide excellent constraints on the binary masses, sky position, and coalescence time with the observational gap of $1\,\mathrm{Hz} \leqslant f_{\mathrm{GW}} \leqslant 10\,\mathrm{Hz}$ between eLISA and Advanced LIGO only spanning ~1 hr. This advance information would allow for optimization of the ground-based detector network, both in terms of active tuning of the detector sensitivity, operational scheduling, and the analysis pipelines, as well as pre-pointing of electromagnetic follow-up telescopes.[4] For the remainder of this section we will focus on detectability and rates for ground-based detectors alone, primarily motivated by the lack of a space-based detector for at least the next decade.

In Figure 6 we show the sensitivity of a network of ground-based detectors to GWs from an IMBH–BH coalescence with non-spinning components with a mass ratio of 10:1, as a function of IMBH mass.

[4] No electromagnetic counterpart is expected from the merger of an IMBH–BH binary in the standard scenario (e.g., Lyutikov 2016), but see Connaughton et al. (2016).

The top panel of Figure 6 shows the horizon distance d_H, which is the luminosity distance at which GWs from a face-on overhead binary would be detected at a signal-to-noise ratio of 8 by a single detector with the sensitivity of Advanced LIGO; the corresponding horizon redshift z_H is shown on the right vertical axis. This signal-to-noise ratio is used as an approximation for sensitivity by the full network (Abadie et al. 2010; Abbott et al. 2016c); the actual sensitivity depends on the network configuration, data quality, and signal duration. We use the noise power spectral density (PSD) of H1 (the LIGO detector in Hanford, WA) during the S6 science run (curve labeled "2010," LIGO Scientific Collaboration 2010b), the measured noise PSD of H1 during the 2015 observing run O1 ("2015–2016," LIGO Scientific Collaboration 2015), low-end predictions for Advanced LIGO noise PSD for the later stages of detector commissioning ("2017–2018," O3 configuration of Abbott et al. 2016), and for design sensitivity runs in the zero detuning, high laser power configuration ("2019+," LIGO Scientific Collaboration 2010a). We use circular effective one-body waveforms calibrated to numerical relativity for signal-to-noise-ratio calculations (Taracchini et al. 2014).

The bottom panel of Figure 6 shows the surveyed detection-weighted comoving volume $\overline{V_c}$

$$\overline{V_c} = \int_0^\infty \frac{dV_c}{dz} f_d(z) \frac{1}{1+z} dz, \tag{17}$$

where $\frac{dV_c}{dz}$ is computed using the Planck (Planck Collaboration et al. 2015) cosmology, $f_d(z)$ is the probability that a binary with the given source-frame masses at redshift z is louder than the signal-to-noise-ratio threshold of 8 (integrated over isotropically distributed sky locations and orientations), and the last factor corrects for the difference in source and observer clocks. With this definition, $\mathcal{R}\overline{V_c}T$ yields the expected number of detections during an observing run with (at least double-coincident) duration T assuming a constant merger rate $\mathcal{R}$ per unit comoving volume per unit source time.

Intermediate mass-ratio coalescences can be observed to a horizon distance of ∼1 Gpc during the O1 science run, and a horizon redshift $z \sim 0.6$ at full design sensitivity. Figure 6 assumes a 10:1 mass ratio. It can be roughly rescaled to other mass ratios by noting that, for a fixed IMBH mass, the signal-to-noise ratio at a given distance, and hence the horizon distance, will scale as $\sqrt{m/M}$ when the signal is inspiral-dominated, and as m/M when the signal is ringdown-dominated. The transition between the two regimes occurs at $M + m \sim 200\ M_\odot$ at Advanced LIGO design sensitivity (see Figure 9 of Haster et al. 2016, which also discusses inference on the parameters of coalescences of intermediate mass-ratio binaries). As a comparison, if the BHs in GW150914 (both BHs in the initial binary and the merger product) had been the lower mass member of a 10:1 mass-ratio IMBH–BH binary, all signals would be ringdown-dominated (Abbott et al. 2016b). The same is valid for the marginally astrophysically significant event LVT151012 (Abbott et al. 2016c) where only the lower mass BH from the initial binary would produce an inspiral-dominated signal.

The IMBH–BH coalescence rate is highly uncertain. Our simulations suggest that around 1 IMBH–BH merger per 10 star clusters is probable in the first ∼ hundred million years of the lifetime of a cluster hosting a suitable IMBH. The merger product may well be ejected from the cluster by the recoil kick from asymmetric GW emission in the last few pre-merger orbits. Assuming that the IMBH is not spinning, the kick velocity for a 10:1 mass-ratio coalescence is $\simeq$60 km s^{-1} (González et al. 2007), comparable to the typical ∼50 km s^{-1} escape velocity from a star cluster. If so, at most ∼ one IMBH–BH merger would happen per cluster before the IMBH is ejected. If the IMBH can increase its mass through other means than BH mergers, e.g., gas accretion in an early time cluster (Vesperini et al. 2010), then the increased mass ratio between the IMBH and the stellar-mass BHs would reduce the likelihood of ejection caused by the recoil kick in the merger.

Even if the merger product is retained, there is a trivial upper limit on the number of mergers per cluster in the Advanced LIGO sensitive frequency band. By the time the IMBH grows beyond several hundred solar masses (see Figure 6), the sensitivity drops significantly; hence, only ∼30 IMBH–BHs per cluster are observable. This limit is also conservative as it assumes IMBH growth only through BH mergers, for an IMBH under gas accretion or runaway collapse of massive stars in a young cluster the number of BH mergers observable by Advanced LIGO before the IMBH mass falls ouside its detectable range would decrease.

Therefore, the IMBH–BH coalescence rate per suitable cluster may vary between 1 and 30 mergers over the cluster's ∼10 Gyr lifetime, or 0.1–3 mergers Gyr^{-1}. The space density of star clusters is ∼3 Mpc^{-3} (Portegies Zwart & McMillan 2000). Following Mandel et al. (2008), we will parametrize the fraction of suitable star clusters (those with the right IMBH mass and central density) by f. Then the total merger rate is in the range $\mathcal{R} \in [0.03(f/0.1), (f/0.1)]$ Gpc^{-3} yr^{-1}. Multiplying this by the surveyed detection-weighted comoving volume, we may expect ∼0.1–5 × $(f/0.1)$ detections per year at full sensitivity. In the near term, 0.01–1 × $(f/0.1)$ detections may be possible during the upcoming O2 6 month observing run, assuming a ∼50% coincident duty cycle.[5]

This calculation may well be optimistic. It assumed a constant merger rate over the cluster lifetime; however, most local star clusters are old (e.g., Kruijssen 2012), and mergers are more likely early in the cluster lifetime. Therefore, most mergers may happen at high redshift, where they are unlikely to be detectable. In addition, the merger rate depends on the cluster inital mass function and its resulting mass segregation effects (Hopman & Alexander 2006). Finally, the fiducial choice $f = 0.1$ is fairly arbitrary; much lower values, including $f = 0$, are possible. On the other hand, if IMBHs are spinning, prograde inspirals could yield higher signal-to-noise ratios, and the detection volume and rate would increase even after averaging over isotropic inspiral orbits (Mandel 2007).

We have also looked for evidence of possible tidal disruptions of stars by the IMBH (see MacLeod et al. 2016, for a recent analysis). Our problem setup is not ideal for this investigation, since we have only two stellar types in addition to the IMBH: 1 solar-mass "stars" and 10 solar-mass "BHs." None of the one-solar-mass stars in our simulation approach the IMBH within the tidal disruption radius. However, if we consider the BHs as proxies for evolving stars, we find that a few would approach within the IMBH tidal disruption radius while in the giant phase of their evolution. Given the gradual hardening of the innermost binary, it is likely that the nominal

[5] These rates should be considered in relation to the upper limits on the rate of binary IMBH coalescences from LIGO–Virgo observations, which are $\geqslant \mathcal{O}(10^3)$ higher depending on the IMBH masses considered (Aasi et al. 2014).

tidal disruption radius would be reached through stellar evolution rather than a dynamically driven encounter. Hence, rather than transient tidal disruptions, we may expect to see Roche lobe overflows, perhaps leading to ultraluminous X-ray binaries such as ESO 243-49 HLX-1 (Farrell et al. 2009; Davis et al. 2011; Godet et al. 2014). In the case of stellar companions additional sources of apsidal precession (for example, precession due to tidal and rotational bulges) may arise and quench LK oscillations similarly to SP as discussed above.

We have also observed a number of ejections of BHs and stars by the binary containing the IMBH. Rapid stellar ejections, particularly at high velocities, could potentially serve as probes for the presence of an IMBH in a cluster.

The capability of our simulation tracking both the complex dynamical features and the merger stands in contrast with previous work such as Leigh et al. (2014), who did not include any pN effects and were thus unable to observe the quenching of LK oscillations due to SP. This could lead to the production of IMBH–BH binaries with artificially long lifetimes as they were unable to merge by the emission of GWs. This issue was partly addressed by MacLeod et al. (2016), who included GW mergers following Peters (1964); however, the interplay of LK effects with SP (and tides in the case of stellar companions) would likely affect their merger rate estimates. Reaching high eccentricities through three-body interactions allows for efficient GW emission at a larger binary semimajor axis as compared to a circular system (Peters 1964; Sesana & Khan 2015). SP-induced freezing of the IMBH–BH orbit at high eccentricities will generally increase the probability that the binary will be highly eccentric after the next three-body interaction, thus facilitating mergers.

Finally, the *N*-body simulations in Leigh et al. (2014), MacLeod et al. (2016), and this work did not include any population of primordial binaries (but see Heggie et al. 2006; Trenti et al. 2007a, 2007b), and while binaries that do not include an IMBH can form dynamically, these would not be specifically tracked. The presence of primordial binary BHs in combination with an IMBH has been shown to affect the retention of BHs in the cluster as well as the evolution of the fraction of BHs in binaries (Pfahl 2005; Trenti et al. 2007b; Leigh et al. 2014), and would thus require a more careful treatment in future studies.

5. CONCLUSION

We have, in a simulation, observed a merger of a $100M_{\odot}$ IMBH and a $10M_{\odot}$ BH within a star cluster as part of the first simulation campaign accounting for post-Newtonian dynamics in the region around the IMBH. This has provided insight into the competitive interplay between pN effects and LK eccentricity oscillations in hierarchical systems as a mechanism for producing and hardening an IMBH–BH binary. We have observed suppression of LK oscillations caused by the pN SP of the IMBH–BH binary giving clear evidence for the necessity of including pN dynamics in future simulations of star clusters to fully capture all relevant dynamical effects leading to the formation, evolution, and merger of an IMBH–BH binary. This is especially relevant toward the end of our simulation, where fast relativistic precession of the IMBH–BH binary freezes its orbit at high eccentricities.

Future extensions to this work will include a larger spectrum of masses (both for the IMBH and the surrounding cluster particles), longer simulation times (requiring further optimization of the code), and additional physical effects (e.g., stellar evolution, a population of primordial binaries, and external tidal fields). We have also commented on the detectability of GWs emitted from an IMBH–BH merger by both space-based and ground-based observatories, with a possible detection within the next decade.

We would like to thank Jonathan Gair, James Guillochon, and Alberto Sesana for useful discussions and suggestions. C.J. H. acknowledges support from CIERA though a visiting predoctoral fellowship and a travel grant from the RAS. F.A. was supported by a CIERA postdoctoral fellowship and from a NASA Fermi Grant NNX15AU69G. We acknowledge the use of computing resources at CIERA funded by NSF PHY-1126812.

REFERENCES

Aarseth, S. J. 2012, MNRAS, 422, 841
Aasi, J., Abbott, B. P., Abbott, R., et al. 2014, PhRvD, 89, 122003
Aasi, J., Abadie, J., Abbott, B. P., et al. 2015, CQGra, 32, 074001
Abadie, J., Abbott, B. P., Abbott, R., et al. 2010, CQGra, 27, 173001
Abbott, B. P., Abbott, R., Abbott, T. D., et al. 2016, LRR, 19, 1
Abbott, B. P., Abbott, R., Abbott, T. D., et al. 2016a, ApJL, 818, L22
Abbott, B. P., Abbott, R., Abbott, T. D., et al. 2016b, PhRvL, 116, 061102
Abbott, B. P., Abbott, R., Abbott, T. D., et al. 2016c, arXiv:1602.03842
Acernese, F., Agathos, M., Agatsuma, K., et al. 2015, CQGra, 32, 024001
Amaro-Seoane, P., & Freitag, M. 2006, ApJL, 653, L53
Amaro-Seoane, P., Gair, J. R., Freitag, M., et al. 2007, CQGra, 24, R113
Amaro-Seoane, P., & Santamaría, L. 2010, ApJ, 722, 1197
Antonini, F., Chatterjee, S., Rodriguez, C. L., et al. 2016a, ApJ, 816, 65
Antonini, F., Hamers, A. S., & Lithwick, Y. 2016b, arXiv:1604.01781
Antonini, F., Murray, N., & Mikkola, S. 2014, ApJ, 781, 45
Antonini, F., & Rasio, F. A. 2016, arXiv:1606.04889
Baumgardt, H., Makino, J., & Ebisuzaki, T. 2004a, ApJ, 613, 1133
Baumgardt, H., Makino, J., & Ebisuzaki, T. 2004b, ApJ, 613, 1143
Berghea, C. T., Weaver, K. A., Colbert, E. J. M., & Roberts, T. P. 2008, ApJ, 687, 471
Berry, C. P. L., & Gair, J. R. 2013, MNRAS, 429, 589
Bode, J. N., & Wegg, C. 2014, MNRAS, 438, 573
Brown, D. A., Brink, J., Fang, H., et al. 2007, PhRvL, 99, 201102
Connaughton, V., Burns, E., Goldstein, A., et al. 2016, ApJL, 826, L6
Damour, T., & Deruelle, N. 1985, AnIHP, 43, 107
Davis, S. W., Narayan, R., Zhu, Y., et al. 2011, ApJ, 734, 111
eLISA Consortium 2013, arXiv:1305.5720
Farrell, S. A., Webb, N. A., Barret, D., Godet, O., & Rodrigues, J. M. 2009, Natur, 460, 73
Gaburov, E., Harfst, S., & Portegies Zwart, S. 2009, NewA, 14, 630
Godet, O., Lombardi, J. C., Antonini, F., et al. 2014, ApJ, 793, 105
González, J. A., Sperhake, U., Brügmann, B., Hannam, M., & Husa, S. 2007, PhRvL, 98, 091101
Graham, A. W., & Scott, N. 2013, ApJ, 764, 151
Gültekin, K., Miller, M. C., & Hamilton, D. P. 2004, ApJ, 616, 221
Gültekin, K., Miller, M. C., & Hamilton, D. P. 2006, ApJ, 640, 156
Hamers, A. S., Perets, H. B., Antonini, F., & Portegies Zwart, S. F. 2015, MNRAS, 449, 4221
Harfst, S., Gualandris, A., Merritt, D., & Mikkola, S. 2008, MNRAS, 389, 2
Haster, C.-J., Wang, Z., Berry, C. P. L., et al. 2016, MNRAS, 457, 4499
Heggie, D. C., Trenti, M., & Hut, P. 2006, MNRAS, 368, 677
Holman, M., Touma, J., & Tremaine, S. 1997, Natur, 386, 254
Hopman, C., & Alexander, T. 2006, ApJL, 645, L133
Huerta, E. A., Kumar, P., McWilliams, S. T., O'Shaughnessy, R., & Yunes, N. 2014, PhRvD, 90, 084016
Innanen, K. A., Zheng, J. Q., Mikkola, S., & Valtonen, M. J. 1997, AJ, 113, 1915
Key, J. S., & Cornish, N. J. 2011, PhRvD, 83, 083001
Konstantinidis, S., Amaro-Seoane, P., & Kokkotas, K. D. 2013, A&A, 557, A135
Kozai, Y. 1962, AJ, 67, 591
Kruijssen, J. M. D. 2012, MNRAS, 426, 3008
Leigh, N. W. C., Lützgendorf, N., Geller, A. M., et al. 2014, MNRAS, 444, 29
Lidov, M. L. 1962, P&SS, 9, 719

LIGO Scientific Collaboration 2010a, Advanced LIGO anticipated sensitivity curves, https://dcc.ligo.org/cgi-bin/DocDB/ShowDocument?docid=2974
LIGO Scientific Collaboration 2010b, H1 Sensitivity, 2010 May 15 http://labcit.ligo.caltech.edu/ jzweizig/distribution/LSC_Data/S6/
LIGO Scientific Collaboration 2015, H1 Calibrated Sensitivity Spectra 2015 Oct 1 (Representative for Start of O1), document number G1501223-v3 https://dcc.ligo.org/LIGO-G1501223/public
Lyutikov, M. 2016, arXiv:1602.07352
Maccarone, T. J., & Servillat, M. 2008, MNRAS, 389, 379
MacLeod, M., Trenti, M., & Ramirez-Ruiz, E. 2016, ApJ, 819, 70
Mandel, I. 2007, arXiv:0707.0711
Mandel, I., Brown, D. A., Gair, J. R., & Miller, M. C. 2008, ApJ, 681, 1431
Mapelli, M. 2016, MNRAS, 459, 3432
Mapelli, M., Huwyler, C., Mayer, L., Jetzer, P., & Vecchio, A. 2010, ApJ, 719, 987
Merritt, D. 2013, Dynamics and Evolution of Galactic Nuclei (Princeton, NJ: Princeton Univ. Press)
Mikkola, S., & Merritt, D. 2006, MNRAS, 372, 219
Mikkola, S., & Merritt, D. 2008, AJ, 135, 2398
Miller, M. C. 2002, ApJ, 581, 438
Miller, M. C., & Colbert, E. J. M. 2004, IJMPD, 13, 1
Miller, M. C., & Hamilton, D. P. 2002, MNRAS, 330, 232
Moore, B., Favata, M., Arun, K. G., & Kant Mishra, C. 2016, PhRvD, 93, 124061
Morscher, M., Pattabiraman, B., Rodriguez, C., Rasio, F. A., & Umbreit, S. 2015, ApJ, 800, 9
Naoz, S., Kocsis, B., Loeb, A., & Yunes, N. 2013, ApJ, 773, 187
Nishizawa, A., Berti, E., Klein, A., & Sesana, A. 2016, PhRvD, 94, 064020
Pasham, D. R., Strohmayer, T. E., & Mushotzky, R. F. 2014, Natur, 513, 74
Pasquato, M., Miocchi, P., Won, S. B., & Lee, Y.-W. 2016, ApJ, 823, 135
Peters, P. C. 1964, PhRv, 136, 1224
Pfahl, E. 2005, ApJ, 626, 849
Planck Collaboration, et al. 2015, arXiv:1502.01589
Portegies Zwart, S. F., & McMillan, S. L. W. 2000, ApJL, 528, L17
Porter, E. K., & Sesana, A. 2010, arXiv:1005.5296
Quinlan, G. D. 1996, NewA, 1, 35
Samsing, J., MacLeod, M., & Ramirez-Ruiz, E. 2014, ApJ, 784, 71
Sesana, A. 2016, PhRvL, 116, 231102
Sesana, A., & Khan, F. M. 2015, MNRAS, 454, L66
Smith, R. J. E., Mandel, I., & Vecchio, A. 2013, PhRvD, 88, 044010
Tanay, S., Haney, M., & Gopakumar, A. 2016, PhRvD, 93, 064031
Taniguchi, Y., Shioya, Y., Tsuru, T. G., & Ikeuchi, S. 2000, PASJ, 52, 533
Taracchini, A., Buonanno, A., Pan, Y., et al. 2014, PhRvD, 89, 061502
Tiwari, V., Klimenko, S., Christensen, N., et al. 2016, PhRvD, 93, 043007
Trenti, M., Ardi, E., Mineshige, S., & Hut, P. 2007a, MNRAS, 374, 857
Trenti, M., Heggie, D. C., & Hut, P. 2007b, MNRAS, 374, 344
Trenti, M., Vesperini, E., & Pasquato, M. 2010, ApJ, 708, 1598
Umbreit, S., & Rasio, F. A. 2013, ApJ, 768, 26
Vesperini, E., McMillan, S. L. W., D'Ercole, A., & D'Antona, F. 2010, ApJL, 713, L41
Vitale, S. 2016, PhRvL, 117, 051102
Wen, L. 2003, ApJ, 598, 419